IL NUOVO CIMENTO Vol. 28 C, N. 2 Marzo-Aprile 2005
DOI 10.1393/ncc/i2005-10179-0

SPH simulations of the waves produced by a falling mass into a reservoir(*)

M. Gallati, G. Braschi and S. Falappi

Hydraulic and Environmental Engineering Department (HEED), Università di Pavia Pavia, Italy

(ricevuto il 7 Febbraio 2005; approvato il 22 Giugno 2005)

Summary. — The characteristics of the waves generated by the falling of a rigid mass or a landslide into a reservoir are simulated via the smoothed particle hydrodynamics (SPH) technique. Specific features are introduced to take care of the dynamic equilibrium of the rigid mass and to deal with the non-Newtonian rheology of the landslide. The validation of the SPH technique, applied to this kind of problems, is first carried out making a laboratory experiment of a circular cylinder sinking into a 2D water tank, in order to ease the boundary problem. Then a more general simulation, suitable to deal with masses with general shape, is applied to a rectangular block falling in a tank filled by two liquids with different density and viscosity. The last simulation reproduces the main characteristics of a landslide occurred in Italy in 1959.

PACS 83.85.Pt – Computational fluid dynamics.
PACS 47.11.+j – Computational methods in fluid dynamics.
PACS 47.85.Dh – Hydrodynamics, hydraulics, hydrostatics.
PACS 01.30.Cc – Conference proceedings.

1. – Introduction

This study is related to the evaluation of the risk due to the falling of masses into a reservoir.

Four stages can be identified in such event: the moving of the solid mass, its impact with the liquid stored in the basin, the generation of a water wave and its propagation in the reservoir.

The flow field produced by the displaced water depends on the typology of the sinking mass (rigid block or landslide), on the volume and the energy of the mass, and in particular on the depth of the water stored in the basin.

(*) Paper presented at CAPI 2004, 8° Workshop sul calcolo ad alte prestazioni in Italia, Milan, November 24-25, 2004.

© Società Italiana di Fisica

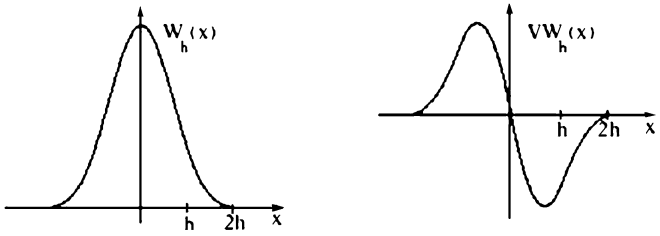

Fig. 1. – 1D kernel function and its derivative.

The motion of the water wave into the basin is the most dangerous effect of the phenomenon. This wave can reach the coasts, damage the towns, and overflow the dam.

After the disasters occurred in the past (Vajont, Pontesei), in Italy a very conservative behaviour is now adopted: the reservoirs under risk are kept almost "empty", with heavy "losses" in energy production, in order to reduce the effect of a possible wave.

Available tools hardly allow realistic estimations of the main characteristics of the water wave to fix the maximum filling of the reservoir compatible with the safety.

Actually the numerical models are regarded as the more promising tools to depict consistent quantitative scenarios relevant to the above risk situation. The numerical model suited for this purpose must be able to deal with strongly unsteady free surface, moving boundaries, interface, non-hydrostatic pressure distribution and non-Newtonian rheology.

Our previous experience [1-3] led us to investigate the possibility of working with the SPH Lagrangian method [4-7], originally developed for astronomical problems. This technique has been recently applied to problems like the vertical sinking of a rectangular block in a tank [8] or the gravity current descending a ramp in a stratified tank [9] and to some non-Newtonian flow [10-12].

The main problems deal with the motion of the masses and their interaction with the liquid volume. In the present paper we only get "in touch" with the question, with the aim of focusing the numerical problems and evaluating the simulation response in view of a deeper analysis. As a first approach the problem is reduced to the 2D vertical Cartesian plane (x, z).

2. – Flow model

The flow generated by the mass displacement into the reservoir is simulated via the SPH technique described in detail in literature [4-7]. As to the particular characteristics of the code developed at HEED and employed for the present simulations reference is made to [1-3]. Later on only the general principles allowing the simulation are recalled.

The SPH technique is based on the numerical approximation of the Navier-Stokes equations on the vertical (x, z)-plane by a kernel interpolation of the variables and assuming a slight compressibility of the fluid.

The material continuum is represented by a distribution of interacting fictitious "particles" with characteristic spatial scale h and fixed mass m. The mass is distributed around the particle centroid according to a kernel function W encompassing a unit volume and with finite support. Figure 1 shows a typical 1D kernel function and its derivative.

Each particle carries velocity $\mathbf{v}$, pressure p, density ρ and other quantities specific

to the flow field. In a generic point of the domain the field variables are expressed as interpolating summations involving the kernel function. For example, the density of a particle i is recovered summing up the contributions of all the j particles belonging to the circular region with radius $2h$ centered at the point:

$$\rho_i = \sum\nolimits_j m_j \, W_{ij} \,, \tag{1}$$

where W_{ij} is

$$W_{ij} \;=\; W\left(\mathbf{r}_{ij}, h\right) \,, \qquad\qquad \mathbf{r}_{ij} \;=\; \mathbf{r}_i \;-\; \mathbf{r}_j \,. \tag{2}$$

Similarly, spatial derivatives at each particle position are evaluated by an interpolating summation involving the derivatives of the kernel function.

With these basic rules and several computational skills not quoted here, the equation of motion written in Lagrangian form [13],

$$\frac{D\mathbf{v}}{Dt} \;=\; -\frac{1}{\rho}\nabla p \;+\frac{1}{\rho}\nabla \cdot \mathbf{T} \;+\mathbf{g} \,, \tag{3}$$

can be discretized for each particle as follows:

$$\left\langle \frac{\mathrm{D}\mathbf{v}}{\mathrm{D}t} \right\rangle_i = -\sum\nolimits_j \frac{m_j}{\rho_i \rho_j} \left(p_i + p_j\right) \nabla W_{ij} + \sum\nolimits_j \frac{m_j}{\rho_j} \left(\frac{\mathbf{T}_j}{\rho_j} - \frac{\mathbf{T}_i}{\rho_i} \right) \cdot \nabla W_{ij} \;+\mathbf{g} \,, \tag{4}$$

where $\mathbf{T}$ is the shear stress tensor.

For a Newtonian fluid the shear stress tensor is proportional to the rate of deformation tensor $\mathbf{S}$ via the dynamic viscosity μ:

$$\mathbf{T} \;=\; 2\mu \, \mathbf{S} \,. \tag{5}$$

For non-Newtonian fluids eqs. (4), (5) could stay formally unchanged providing that an effective viscosity μ_{eff} is defined for each particle [10, 11]. This effective viscosity must be evaluated in agreement with the rheological properties of the material and the interpolated strain rate value of the particle as follows [14]:

$$\mu_{\mathrm{eff}} = \frac{\tau_c}{\sqrt{I_{2(S)}}} + K \left(\sqrt{I_{2(S)}} \right)^{n-1} \,, \tag{6}$$

where τ_c is the yield stress, K is the consistency, n the exponent of the rheological curve and $I_{2(s)}$ is the second invariant of the rate of deformation tensor.

The continuity equation written in Lagrangian form [13],

$$\frac{\mathrm{D}\rho}{\mathrm{D}t} = -\rho \, \nabla \cdot \mathbf{v} \,, \tag{7}$$

is discretized as follows:

$$\left\langle \frac{\mathrm{D}\rho}{\mathrm{D}t} \right\rangle_i = \sum\nolimits_j m_j \left(\mathbf{v}_i - \mathbf{v}_j\right) \cdot \nabla W_{ij} \,. \tag{8}$$

Assuming a slight compressibility of the fluid the pressure of each particle can be evaluated by providing its equation of state in a simplified form [7]:

$$p_i = c^2 \, (\rho_i - \rho_0) \ , \tag{9}$$

where ρ_0 is the reference value for the density of the material continuum and c is the speed of sound.

The continuum is discretized by a set of particles using a proper spatial scale h. At the starting time position, mass, velocity, pressure and density are therefore fixed for each particle according to the initial state of the system.

To reach the system configuration at following time steps we adopt an explicit staggered scheme. This choice compels us to enforce the Courant and the Prandtl conditions on the time step to get the numerical stability. The time step δt is related to the spatial scale h by the equation

$$\delta t \leqslant \ \alpha \ \min \left\{ \frac{h}{c + |\mathbf{v}_{\max}|} \ , \ \frac{h^2 \, \rho}{2 \, \mu} \right\}, \tag{10}$$

where α is a numerical coefficient and $\mathbf{v}_{\max}$ is the maximum value of the velocity. The sound speed must be chosen carefully to ensure an efficient and accurate solution of the problem. In order to increase the time step it is possible to take the value of the sound speed lower than the real one, but high enough so that the Mach number of the flow is lower than 0.1 [6, 7]. The effective viscosity in eq. (6) attains an infinite value when $I_{2(s)}$ tends to be infinitesimal. Such large value of viscosity will strictly reduce the time step and create numerical divergence. Thus the effective viscosity is numerically bounded by a fixed high value usually 10^3 times larger than consistency K to ensure convergence and a reasonable time step [11].

The proper boundary conditions should be applied on the borders of the domain in order to mimic the absence of flux through the boundary and to control the slip of the fluid. Via the image particle method the boundary effects are ensured creating an image particle for each particle of the continuum whose distance from the borders is less than $2h$. The image particle is placed outside the domain reflecting the starting particle position through the borders. This particle has the same density and pressure of the continuum particle, while the normal component of the velocity has opposite direction.

Different slip conditions could be applied along the boundary. The choice of the boundary condition depends on the number of particles used to describe the continuum, the properties of the material and the geometrical shape of the boundaries. The physical no-slip condition requires a spatial scale of the particles small enough to accurately represent the velocity gradient in the boundary layer. This could require a great number of particles to discretize the material continuum and so a high computational cost. In such a situation it would be better to apply a controlled slip condition assigning the value of local tangential stress, computed via the boundary-layer approximation.

The new problems worked out in the present study deal with the simulation of dynamics of the mass.

Two strategies have been implemented for the rigid masses.

In the first strategy, suitable for regular form of the falling mass, the block is simulated through its moving boundaries. The boundaries shape stays unchanged during the simulation, while their positions are computed and updated at every time step via the global dynamic equilibrium of the mass itself. This is obtained balancing the inertial

force to the weight of the block and the force acted on the block by the fluid due to pressure and tangential stresses. Such variables are computed at each time step on the borders of the block and properly integrated to produce the required forces. The free-slip boundary condition, enforced via the particle method, is applied.

In the second strategy, useful for masses with general form, the sinking block is discretized by a set of particles. The individual motion of the block particles is computed according to the general strategy presented above, summing up the contributions of all the particles, either the ones of the block and the ones of fluid, belonging to the circular region with radius $2h$.

Moreover a rigidity constraint is applied to the block particle through inner forces, controlled by the local deformation, in order to reproduce the non-deformability of the mass. Because of the mutual interactions of the block and the water particles no additional boundary condition is needed on the borders of the block itself.

The last problem deals with the landslide simulation. We represent the landslide by a set a particles with proper mass and density and a proper constitutive equation that defines a stress-strain rate relation for the material.

Also for each landslide particle the discretized flow equations must be solved summing up the contributions of all the particles, both the landslide and the water ones, belonging to the circular region with radius $2h$.

Landslides exhibit non-Newtonian behaviour; this implies that a rheological model should be chosen according to the material properties. As shown above the discretized Navier-Stokes equations could stay unchanged providing the definition of an effective viscosity for each particle in agreement with the rheological properties of the material and the interpolated strain rate value.

3. – Vertical sinking of a cylinder in a water tank

The following case is a simulation of an experiment carried out at the HEED Laboratory. We applied here the first strategy of rigid mass-water interaction.

In the experiment the aluminium block of circular shape is forced to sink along the center line of the tank. The tank is built connecting two plexiglas walls on a frame 0.03 m thick to ensure in any case the main 2D characteristics of the flow field. The structure is provided by vertical grooves along which two pins connected with the cylinder can slide thus assuring the absence of rotation. The cylinder is instantaneously released from its initial position and the whole flow field is recorded by digital videocamera at 25 frames per second. The test is repeated several times and the images are then processed to get the instantaneous water profile of every frame.

The experimental setting can be seen in the first frame of fig. 2: the tank is 0.5 m long, the water depth is $H_t = 0.28$ m, and the circular aluminium block has a diameter of 0.155 m.

The main characteristics of the phenomenon are summarized in the record of first and third row of fig. 2.

The initial rest field has been schematized by a set of particles placed according to a regular grid with a step equal to 0.0033 m, with a corresponding number of particles of ~ 11000. The kernel scale $h = 0.004125$ m is adopted. A free-slip boundary condition is adopted for the walls and bottom of the tank and for the sinking block. The computation time step is $\sim 10^{-4}$ s in order to fulfill the stability conditions.

Starting from the initial state the block accelerates toward the bottom thus displacing laterally and upward the water that meets along its path. The two lateral streams meet in

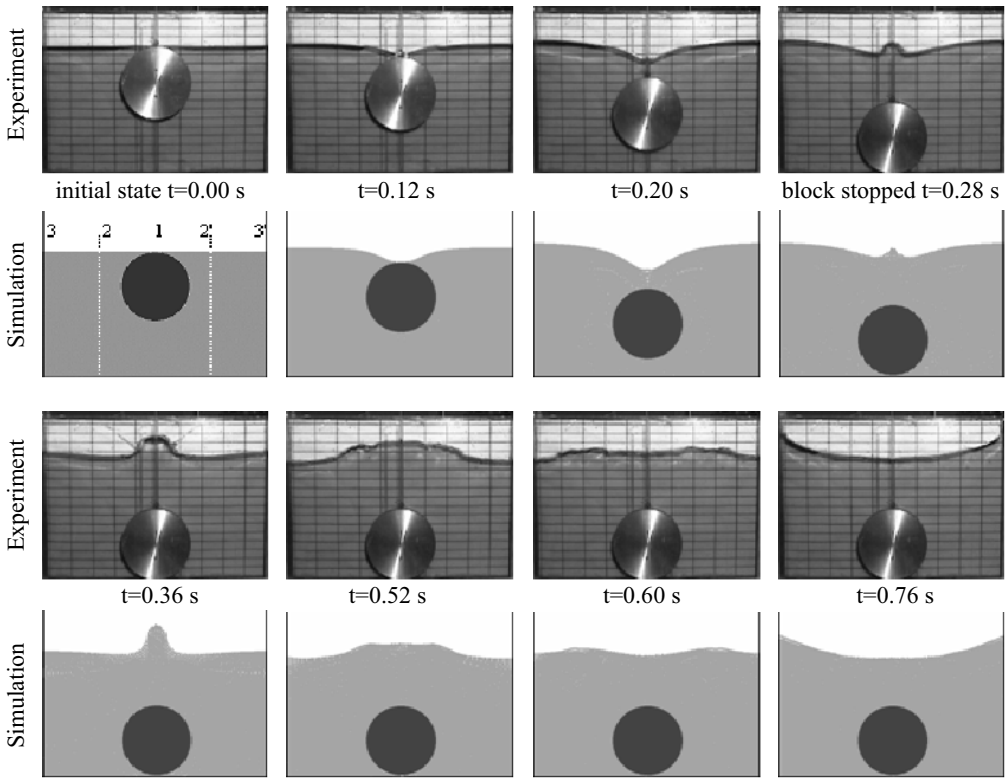

Fig. 2. – Recorded frames and corresponding simulation pictures.

the rear part of the cylinder forming a wave with maximum at the center line of the tank. The wave propagates toward the walls, reflects and gives rise to a stationary wave. When impacts of the two streams or against walls occur, air entrapment and perturbations at a scale lower than the tank thickness take place and the liquid mass eventually breaks in drops and splashes: we expect that such highly nonlinear and multiphysics phenomena are not captured by the simulation, strictly based on a 2D schematization of the liquid.

The comparison between computed and observed fields shows that the main characteristics of the flow are captured regarding both the free-surface shape and at the sinking times and velocity.

The simulation performed with a PowerPC G4 867 MHz desktop computer took about 8 h.

4. – Free sinking of a rectangular block in a tank

Similar results of those above described are achieved with the second strategy.

To show the ability of the code in dealing with very complex phenomenon we present here the simulation of a rectangular sinking block starting with a given spin at $t = 0$ s, falling into water overlying a layer of high-density fluid.

The fluid in the lower side of the tank (5m long) has density 1800 kg/m^3 and viscosity $\mu_{\mathrm{b}} = 10^{-2}$ Pa·s. The depth of this fluid is $H_{\mathrm{b}} = 0.3$ m, while the thickness of the water

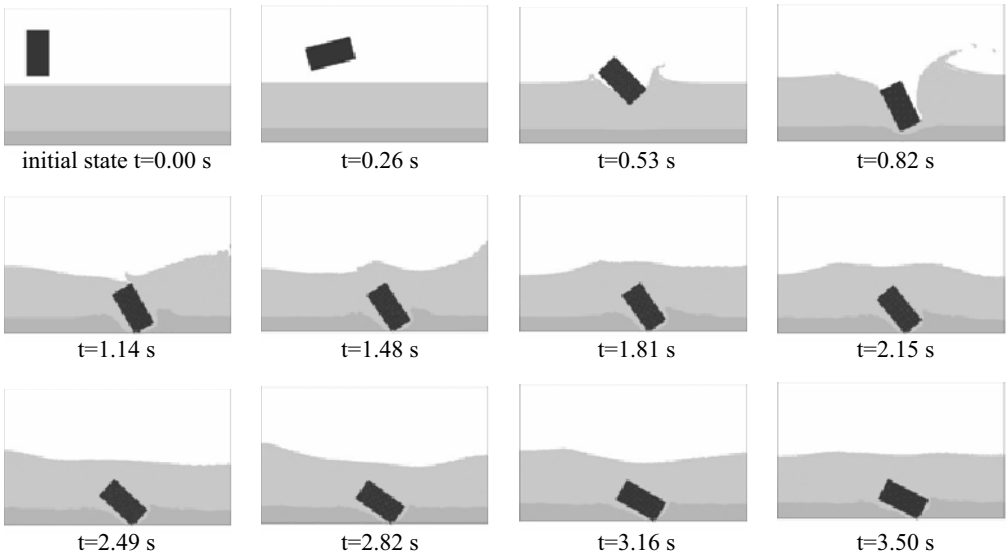

Fig. 3. – Simulation pictures.

layer is $H_{\mathrm{w}} = 1$ m. The rectangular block has width $L_{\mathrm{r}} = 0.5$ m, height $H_{\mathrm{r}} = 1$ m and density 1500 kg/m^3. The horizontal and vertical components of the initial speed are 3 m/s and 1 m/s, while the initial spin is 5 rad/s.

The initial field is represented by a set of particles regularly placed on a square grid of step 0.033 m, with a corresponding number of particles of ~ 6000. The kernel scale $h = 0.0375$ m is adopted.

Free-slip boundary conditions are assumed for the walls and bottom of the tank.

The computation time step is $\sim 10^{-3}$ s in order to fulfill the stability conditions.

The main characteristics of the simulation are displayed in fig. 3.

Starting from the initial state the block moves according with the initial conditions and the gravity acceleration. Two asymmetrical waves are generated in the tank by the impact of the block on the water surface. These waves spread all over the domain, and are reflected by the lateral surfaces of the tank.

The block moves through the liquid in the tank generating pressure waves that deform the high-density fluid before the reaching of the block itself. Carrying on the simulation the waves interact reducing their amplitudes, while the block reaches the bottom of the tank and then stops in a sloping position because of the higher density of the fluid below.

Looking at the images above, we think that the obtained results should agree with the real phenomenon, even though a comparison between the simulation and an experiment is not available.

The simulation, performed with a PowerPC G4 867 MHz desktop computer, took about 1 h, completing ~ 2000 steps with a CPU time of ~ 1.8 s for each step.

5. – Simulation of Pontesei landslide

The third example deals with the simulation of the impact effect of a landslide in a basin. It is scaled on a phenomenon occurred in Italy in March, 1959: a great landslide

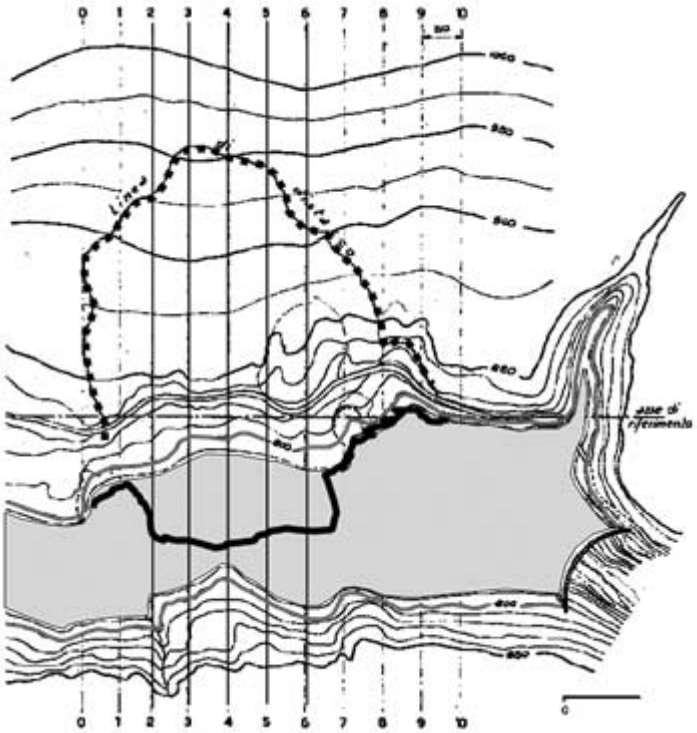

Fig. 4. – Basin plan.

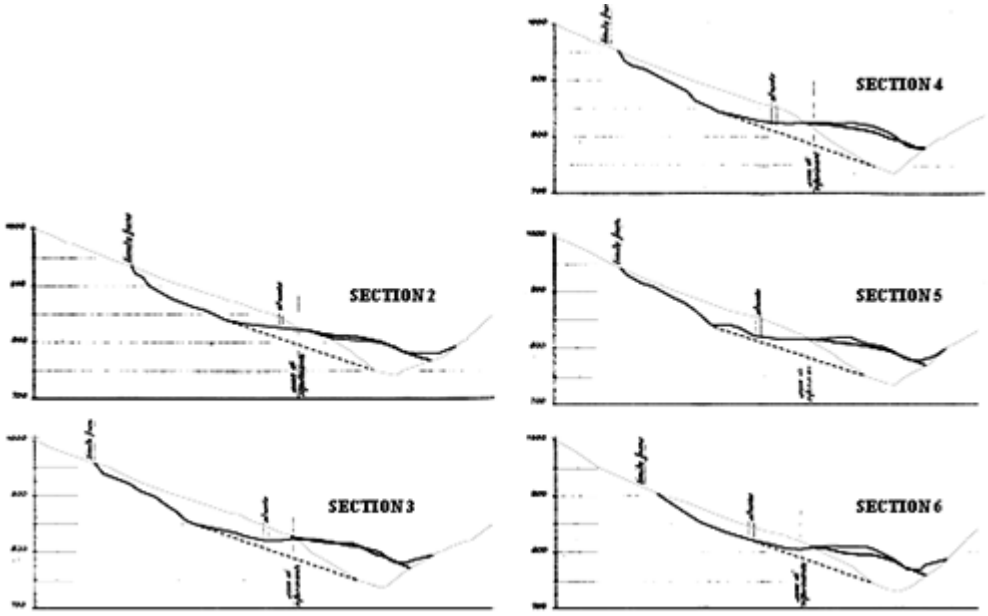

Fig. 5. – Ground profiles measured in the different sections before and after the landslide.

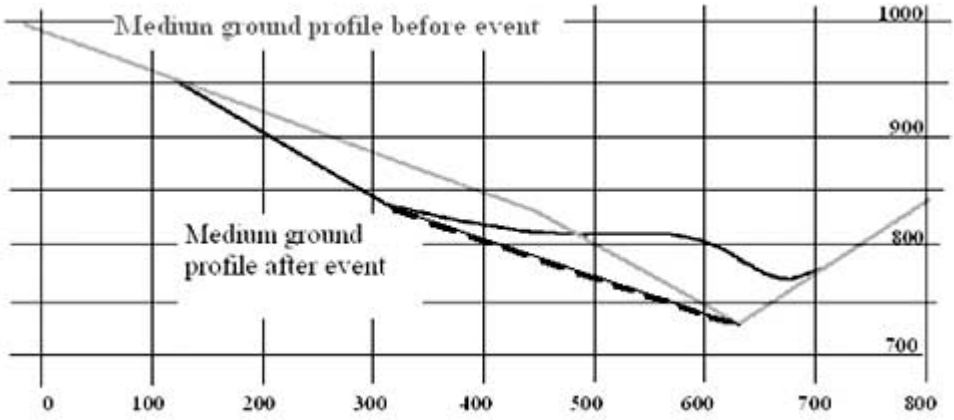

Fig. 6. – Medium ground profiles before and after the landslide.

fell into the hydroelectric basin of Maè in Pontesei, displacing a large volume of water and creating a wave that overtopped the dam.

The plan of the basin is reproduced in fig. 4. The grey area represents the water surface just before the landslide. The vertical lines identify the sections in which the ground profile has been measured before and after the event. Separation line is represented with a dotted line, while the landslide front after the event is represented by the continuous line. Looking at this image it could be noticed that the solid mass flow did not show significant lateral spreading.

The images in fig. 5 are the ground profiles measured before and after the event in the different sections (2-6). Taking the average of the measured ground profiles it is possible to identify a medium profile of the ground before and after the event as shown in fig. 6. These medium profiles represent the initial geometrical configuration of the landslide used as the input for the simulation, and the final situation, needed to check the simulation results.

The similarity of the measured profile in the sections partially justifies the use of the 2D approach to this problem. We do not miss accuracy in the description of the landslide, but, as evident, the water flow would need a 3D description because of the propagation of the generated waves in all the directions.

The Bingham rheological model has been used to describe the landslide. The parameters of the model are set looking at the most common values used in literature [10, 15]. We take 1500 Pa for the yield stress, 1000 Pa$\cdot$ s for the consistency and 2000 kg/m^3 for the density.

The water level is set at 787 m above the sea level. This was the real filling of the basin before the event.

In the simulation the initial field is represented by a set of particles regularly placed on a square grid of step 2.0 m, with a corresponding number of particles of ~ 5600. The kernel scale $h = 3.0$ m is adopted.

We impose a no-slip boundary condition for the landslide and a free-slip condition for water.

The computation time step is ~ 0.015 s in order to satisfy the stability conditions.

Figure 7 shows the simulation result from the original failure of the slope.

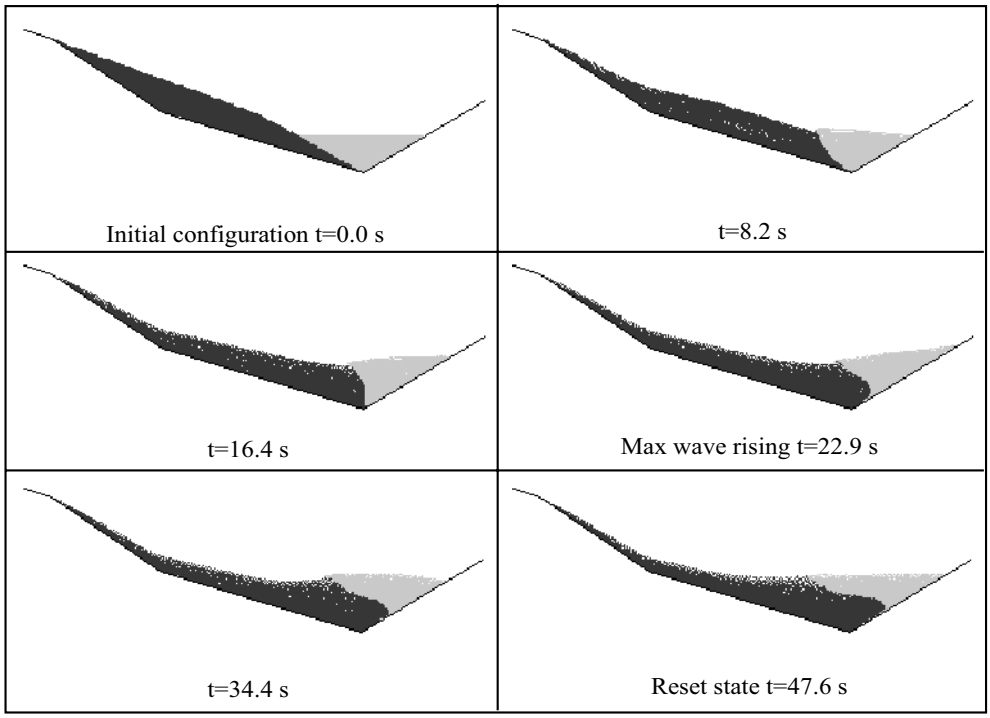

Fig. 7. – Different stages of the simulation.

The landslide flow displaces the water stored in the basin, generating a wave that runs up the right slope. The maximum run up level is reached at 22.9 s. The water wave goes back and partially overtop the landslide before the system comes to a rest state at 47.6 s.

In fig. 8 the final profile obtained from the simulation is compared with the measured medium profile after the event, represented by the hatched line.

This image shows an acceptable agreement between the simulated and the observed profile, while the run up level of the water wave is probably fairly overvalued, because of the 2D approach.

Fig. 8. – Final profile of the simulation compared with the measured medium profile after the event.

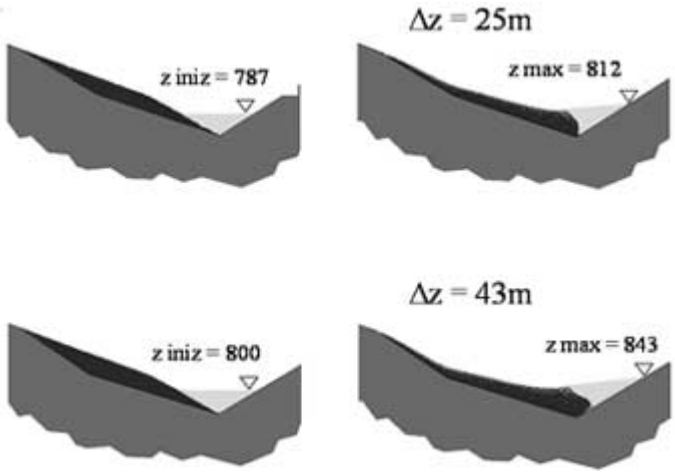

Fig. 9. – Maximum run up height with two different fillings.

To exemplify the flexibility of the numerical methods in depicting different scenarios we computed the maximum level reached by the wave with a different filling of the basin (800 m above the sea level). The images in fig. 9 show how the maximum run up height increases in a nonlinear way when increasing the water level in the basin.

The simulation, performed with a PowerPC G4 867 MHz desktop computer, took about 3 h, completing ~ 3200 step with a CPU time of ~ 3.0 s for each step.

6. – Conclusions

The SPH model exhibits a remarkable aptitude for reproducing the phenomena considered in this paper, involving both a rigid body sinking in a tank and a landslide fall. In all the situations analyzed the results obtained by the simulations are in reasonable agreement with the laboratory data or the field observations. Even if in this paper we only get in touch with this kind of problems and other validations are needed we regard this technique as a very promising and flexible tool.

The parallelization of the code and the implementation of the 3D model will be the next steps of the research.

The parallelization of the code will enable us to make the most from the super calculators power, and so maintain short the computational time required by simulations also increasing the number of particles to refine the accuracy of the results. Because of the code structure, we think that the parallelization will be very efficient on a shared memory calculator: the main operation required is the allocation of a fixed number of particles to each processor. Otherwise using a distributed memory calculator the parallelization requires more operations like a dynamic domain decomposition to reach a correct balancing of the different processors during the simulations.

The 3D scheme is necessary to simulate problems, like the propagation of the water waves in Pontesei basin, that cannot be reduced to a 2D scheme. As shown above the basic equations of the SPH technique are already written in a 3D form. The main problem is related to the high computation time required for a 3D simulation. In fact a great number of particles is usually required for a 3D simulation, moreover the number of inter-

acting particles increases. To have an acceptable computational time the parallelization is required.

REFERENCES

[1] Gallati M. and Braschi G., *L'acqua*, **5** (2000) 7.
[2] Gallati M. and Braschi G., *Proceedings of IASTED International Conference on Applied Simulation and Modelling, 2002, Crete, Greece* (Acta Press) 2002, pp. 530-535.
[3] Gallati M. and Braschi G., *Proceedings of the International Conference on Fluid Flow Technologies (CMFF'03), 2003, Budapest, Hungary*, edited by Lajos T. and Vad J., 2003.
[4] Monaghan J. J. and Gingold R. A., *J. Comput. Phys.*, **52** (1983) 374.
[5] Monaghan J. J., *J. Comput. Phys.*, **82** (1989) 1.
[6] Monaghan J. J., *J. Comput. Phys.*, **110** (1994) 399.
[7] Morris J. P., Fox P. J. and Zhu Y., *J. Comput. Phys.*, **136** (1997) 214.
[8] Monaghan J. J. and Kos A., *Phys. Fluids*, **12** (2000) 622.
[9] Monaghan J. J., Cas R. A. F., Kos A. and Hallworth M., *J. Fluids Mech.*, **379** (1999) 39.
[10] Rodriguez-Paz M. X. and Bonet J., *Numer. Methods Partial Differential Eq.*, **20** (2004) 140.
[11] Shao S. and Lo E. Y. M., *Adv. Water Res.*, **26** (2003) 787.
[12] Lachamp P., Faug T., Naaim M. and Laigle D., *Nat. Hazard Hearth Sys. Sci.*, **2** (2002) 203.
[13] Schilchting H., in *Boundary-Layer Theory* (McGraw-Hill, N.Y.) 1979.
[14] Oldroyd, in *Rheology*, edited by Eirich F. R., Vol. **1** (Academic Press, New York) 1956.
[15] O'brien J. S. and Julien P. Y., *J. Hydraulic Engin.*, **118** (1988) 877.